Magnetic interactions in the ludwigite Ni$_2$FeO$_2$BO$_3$

J. C. Fernandes, R. B. Guimarães, and M. A. Continentino

Instituto de Física, Universidade Federal Fluminense Campus da Praia Vermelha, Niterói, 24.210-340, RJ, Brazil

H. A. Borges

Departamento de Física, Pontifícia Universidade Católica do Rio de Janeiro, Rio de Janeiro, 22452-970, RJ, Brazil

A. Sulpice

Centre de Recherches sur les Très Basses Temperatures-CNRS 25, Av. des Martyrs, BP 166, 38042 Grenoble Cedex 9, France

J-L. Tholence

Laboratoire des Propriétés Electroniques des Solides-CNRS 25, Av. des Martyrs, BP 166, 38042 Grenoble Cedex 9, France

J. L. Siqueira, L. I. Zawislak, J. B. M. da Cunha, and C. A. dos Santos

Instituto de Física, Universidade Federal do Rio Grande do Sul, Av. Bento Gonçalves, 9500, Porto Alegre, 91501-970, RS, Brazil

We present an investigation of the magnetic properties of the ludwigite Ni$_2$FeO$_2$BO$_3$. This material is an oxyborate that presents in its crystalline structure subunits in the form of walls where the transition metal ions are located. Our Mössbauer, ac susceptibility, and magnetization measurements show that Fe and Ni ions form two independent subsystems in this material down to $T_N = 15$ K. We explain this behavior in terms of a hierarchy of interactions. [S0163-1829(98)01325-3]

I. INTRODUCTION

The oxyborates form a family of compounds having several chemical compositions and *circa* ten known different crystalline structures.[1–6] Those having general chemical formula $M^{2+}M^{3+}OBO_3$ crystallize as *warwickites*, while the *ludwigites* have a general formula $M_2^{2+}M^{3+}O_2BO_3$. The other structures, more complex, require chemical formulas that deviate moderately from that of the ludwigites in order to be stabilized. All the crystalline structures of the oxyborates are quite similar: the divalent and trivalent metals, M^{2+} and M^{3+}, which may be either the same or different metal ions, are found at the centers of edge-sharing oxygen coordination octahedra. The boron ions remain at the centers of oxygen coordination triangles, each corner of which is a corner of a different octahedra. The chemical composition of such materials, their synthesis and crystallographic parameters have been extensively studied. Recently it has been shown that the warwickites behave from the magnetic[7–10] and electronic[11–13] point of view as essentially one-dimensional (1D) materials. This is due to the hierarchy of the interactions in their structures that consist of subunits in the form of ribbons.

These results led us to extend our investigation of the physical properties of the oxyborates and to study the magnetic properties of the ludwigite Ni$_2$FeO$_2$BO$_3$. This material can also present low-dimensional magnetism due to its structural similarity with the warwickites. In the present case however the relevant subunits are *walls* rather than ribbons (see Fig. 1). The crystalline structure of ludwigites is orthorhombic. Its space group is V_h^9-*Pbam*. Columns of edge-sharing octahedra form zigzag walls parallel to the c axis as shown by the polyhedral drawing of the ludwigite structure

in Fig. 1. Lattice parameters for some ludwigites are shown in Table I. The main chemical bonds between walls are due to the boron ions: the trigonal borate group BO_3^{3-} is the strongest bonded group of ions in the oxyborates.[11] In the ludwigite Mg$_{1.93}$Mn$_{1.07}$O$_2$BO$_3$ the metal positions 1, 2, 3, and 4 (see Fig. 1) have a trivalent ion Mn^{3+} content of 14%, 34.6%, 72.6%, and 9.8%, respectively.[2] Approximately the same occupancies are expected for the trivalent ion Fe^{3+} in the Ni$_2$FeO$_2$BO$_3$ ludwigite as is the case of warwickites that
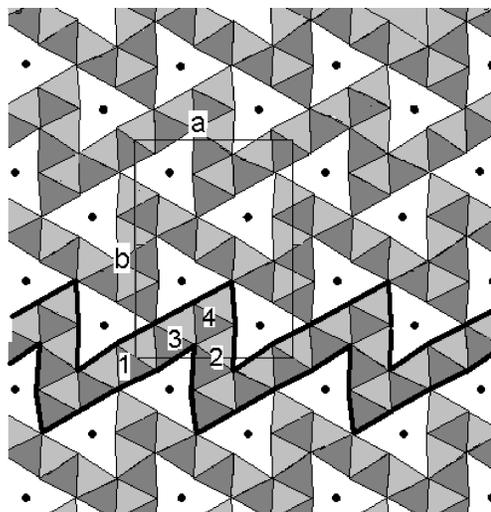
FIG. 1. Schematic polyhedral drawing of the ludwigite structure viewed along the c axis. The a axis is horizontal and the b axis is vertical. The unit cell and the atom numbering used for the metal positions are indicated. The black circles represent the boron ions. One of the subunits, we call *walls* in the text, is bordered by bold lines. See Ref. 2.

TABLE I. Cell unit parameters of some ludwigites; (*) - natural material; (**) - present work.

	a(Å)	b(Å)	c(Å)	Ref.
$Ni_2FeO_2BO_3$	9.209(4)	12.232(5)	3.002(1)	(**)
$Ni_2FeO_2BO_3$(*)	9.213(4)	12.229(5)	3.001(1)	15
$Mg_2MnO_2BO_3$	9.202(2)	12.532(2)	2.993(1)	2
$Ni_2CrO_2BO_3$	9.209(1)	12.121(1)	2.9877(3)	5
$Ni_2VO_2BO_3$	9.199(2)	12.211(2)	2.988(1)	5

keep the same relative occupancies from one chemical formula to another. In fact, we will confirm this further on in this paper. It is clear then that the oxyborates are naturally disordered materials and this is an essential ingredient to understand their physical properties. A detailed description of the ludwigite structure may be found in Ref. 2.

Note that inside each wall the distances between the magnetic ions are such that direct exchange between the 3D electrons is the dominant one (Table II). The interaction between two neighboring ions in adjacent walls is mainly due to superexchange through the oxygen ion at the only common corner of the respective coordination octahedra. For this reason it should be expected that the ludwigites behave as a 2D magnetic system. The 1D magnetism arises in the warwickites since the walls in these systems are reduced to ribbons four columns wide.

This paper reports susceptibility, magnetization and Mössbauer spectroscopy (MS) measurements in a powdered sample of $Ni_2FeO_2BO_3$. Also, the x-ray identification of the crystalline structure of the sample is presented. The results of our magnetic measurements indicate that the Fe and Ni *sublattices* behave as two decoupled subsystems of spins down to 15 K. Within each subsystem the coupling is essentially antiferromagnetic since there is no macroscopic magnetization. The 3D ordering of the iron and nickel subsystems occur at 106 and 46 K, respectively. We have verified that the nickel subsystem in this compound presents a behavior characteristic of random exchange Heisenberg antiferromagnetic chains (REHAC) above its 3D ordering temperature, $T_N^{Ni} \approx 46$ K, as is also observed in the warwickites.[10] For the Fe subsystem the 3D ordering at $T_N^{Fe} = 106$ K is probably of the spin-glass type as in most dilute random magnetic systems with antiferromagnetic couplings. This is indeed the case for the ludwigite $Mg_2FeO_2BO_3$.[14]

II. SAMPLE PREPARATION AND CHARACTERIZATION

The sample was synthesized from a stoichiometric mixture of the oxides NiO and Fe_2O_3 in borax. The mixture was

TABLE II. Distances between metallic neighbors sites in $Ni_2FeO_2BO_3$.

Metal sites	Distance Å	Relative situation
1 - 3	3.088	intrawall
1 - 4	3.363	interwall
2 - 3	2.691	intrawall
2 - 4	3.136	intrawall
3 - 4	3.066	intrawall
3 - 4	3.381	interwall
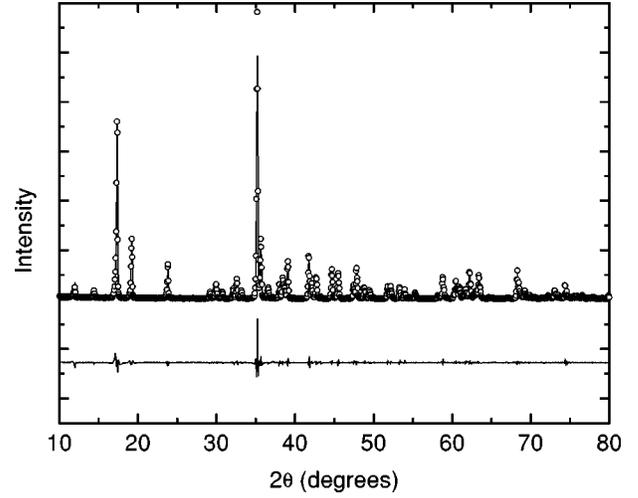
FIG. 2. Room-temperature x-ray powder-diffraction pattern for $Ni_2FeO_2BO_3$. The open circles represent the observed data. The solid line represents the calculated pattern obtained from the Rietveld refinement. The lower trace is a plot of the residual spectrum, i.e., the difference between experimental and calculated intensities.

heated at 1050 °C in pure oxygen atmosphere during two days and, then, slowly cooled. A black powder was obtained whose grains were about 100 μm long.

Its x-ray-powder diffraction (XRPD) pattern was recorded from a Siemens D 5000 diffractometer using a curved graphite monochromated Cu$K\alpha$ radiation. A scan step of 0.02° in the 2θ range from 10° to 100° was carried out under a fixed counting time of 4 s. Structural refinement, to be reported elsewhere, was done using the program FULLPROF. [16] The XRPD pattern, shown in Fig. 2, was indexed to the space group *Pbam* with unit-cell parameters similar to those previously reported. Table I shows the cell parameters obtained from this and from other experiments. The good quality of the sample, without signs of spurious phases, is verified by the small intensities of the residual spectrum also shown in Fig. 2.

III. MEASUREMENTS

A. Magnetic susceptibility

The real part of the ac susceptibility of $Ni_2FeO_2BO_3$, χ_{ac}, measured at 125 Hz in a Lake-Shore apparatus, is shown in Fig. 3. It may be remarked that, besides the intense peak located at 46 K, there is a weak one at 106 K. Also, an abrupt change of the derivative may be observed at 15 K. At this same temperature a peak is observed in the M/H vs T and M vs T curves, as will be shown below. The intense peak position at 46 K does not change with measuring frequency in the range 20–1000 Hz. This result rules out a spin-glass nature for such a transition that can be identified, as we argue further on, with the 3D antiferromagnetic ordering of the Ni subsystem. The inset in Fig. 3 shows the logarithmic plot of a segment of the $\chi_{ac}(T)$ curve. It is clear that, for 50 K< T<75 K, $\chi_{ac} \propto T^\alpha$ where $\alpha = -0.73$. This behavior is characteristic of REHAC,[7,8,10] which in the present case are Ni chains.
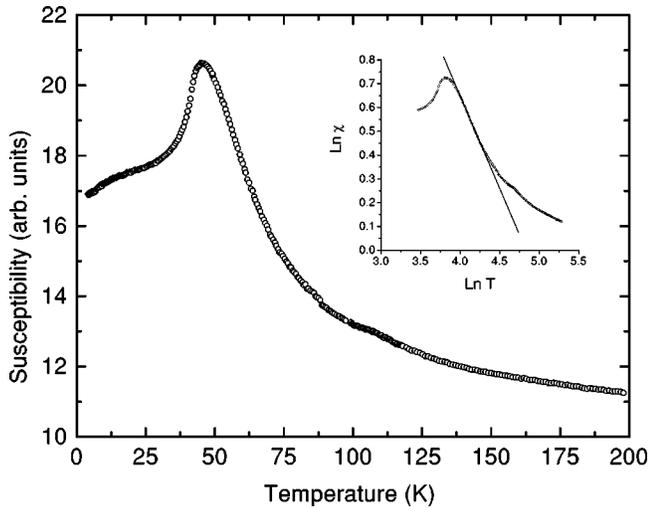
FIG. 3. ac magnetic susceptibility of $Ni_2FeO_2BO_3$, χ_{ac}, measured at 125 Hz under an oscillating applied field of 10 Oe. Inset: Plot of $\ln \chi_{ac}$ vs $\ln T$ for a segment of the total measured curve.

FIG. 5. Magnetization vs temperature curve, under an applied field of 5 T, for $Ni_2FeO_2BO_3$. The splitting is due to FC and ZFC regimes. A small peak near 15 K in the ZFC curve may be observed.

B. Magnetization

Magnetic measurements were performed using a superconducting quantum interference device magnetometer in the temperature range from 4 to 60 K and in fields from $H = 0T$ to $H = 7.5$ T. We have measured the magnetization M as a function of field H for fixed temperatures. From these isotherms we have obtained curves M/H vs T for different applied magnetic fields H. Some of these curves are shown in Fig. 4. They present two anomalies, which for $H = 0$ occur at $T_N^{Ni} = 46$ K, the same temperature of the intense peak in χ_{ac}, and $T_N = 15$ K where the derivative of $\chi_{ac}(T)$ changes abruptly. The peak temperature identified as T_N^{Ni} shifts to lower temperatures as the applied magnetic field increases, while the low-temperature peak is field independent within the precision of the measurements. Curves of M vs T for two

different histories, field cooled (FC) and zero-field cooled (ZFC), are shown in Fig. 5 and present irreversibility or history-dependent effects starting above $T_N^{Ni} = 46$ K. The magnetization curve obtained at $T = 4$ K is shown in Fig. 6. It does not show any significant hysteresis or remanent magnetization. Figure 7 shows the temperature of the peak in the curves of M/H vs T as a function of the applied magnetic field H.

C. Mössbauer spectroscopy

MS measurements were performed between 4.2 K and 300 K. The spectra were taken using a constant acceleration electromechanical drive system with a multichannel analyzer for collecting and storing the data. The temperature stability was better than 0.1 K. [57]Co in rhodium was used at room temperature as the source, with a nominal activity of 20 mCi. The hyperfine parameters for the paramagnetic spectra were obtained by a least-squares procedure assuming Lorentzian line shapes constrained to equal halfwidths. Following the Window model,[17] the spectra obtained in the magnetically

FIG. 4. Magnetic susceptibility (M/H) vs temperature curves for $Ni_2FeO_2BO_3$ obtained from the isothermal magnetization curves for three values of the applied magnetic field. A small peak near 15 K may be observed. The continuous lines are guides for the eyes. The dashed lines are Lorentzian fits to each field value to determine the corresponding peak position, $T_p(H)$. These points are plotted in Fig. 7. The error in each experimental point is less than 1/1000 of the (M/H) value.

FIG. 6. Magnetization vs applied field curve for $Ni_2FeO_2BO_3$ at 4 K showing the very small hysteresis and magnetization of the system.
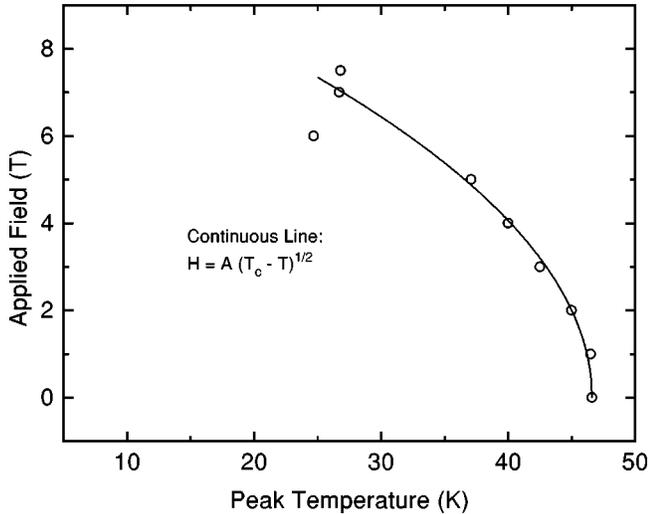
FIG. 7. Temperature of the intense peak in the (M/H) curve vs applied field for $Ni_2FeO_2BO_3$. The points are taken from the M/H vs T curves (see Fig. 4). The continuous line represents the function $H = A(T_N^{Ni} - T)^{1/2}$ fitted to the experimental points.

ordered regime were fitted to a hyperfine field distribution (HFD), $p(H_M)$, by superposing subspectra with Lorentzian line shapes, constrained to equal quadrupole splitting, isomer shift and halfwidths. Typical errors are $\pm 3\%$ on hyperfine parameters and $\pm 5\%$ in site occupancies.

At room temperature, four symmetrical doublets (see Fig. 8), with hyperfine parameters displayed in Table III, represent the paramagnetic regime. All the doublets could be fitted to isomer shift values relative to αFe smaller than 0.4 mm/s, characteristic of Fe^{3+}. However, all the fitted quadrupole splittings could be attributed to both Fe^{2+} or high spin Fe^{3+}. We attributed the four doublets to high spin Fe^{3+} since the isomer shift is more sensitive to the oxidation state than the quadrupole splitting. Such a behavior has been observed in $RbFeF_4$ and $KFeF_4$.[18] The site assignment displayed in Table III was based on the structural refinement. It may be remarked, from Table III, that the Fe^{3+} occupancies found for each site in $Ni_2FeO_2BO_3$ are very near those found for the Mn^{3+} ion in the ludwigite $Mg_{1.93}Mn_{1.07}O_2BO_3$.
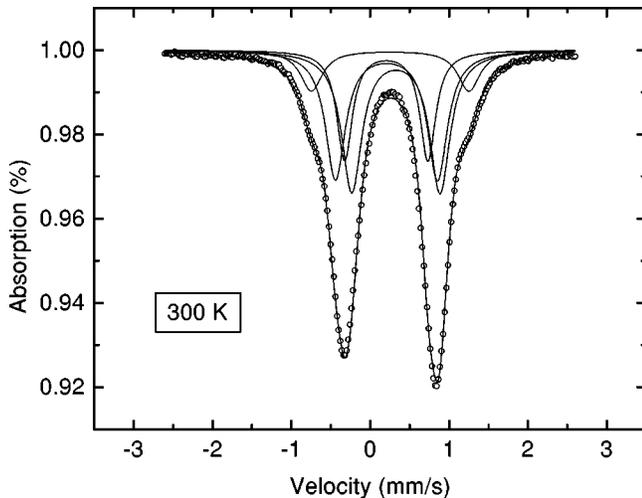
FIG. 8. Room-temperature Mössbauer spectrum from $Ni_2FeO_2BO_3$ (circles). The continuous curves represent the fitted spectra for each one of the four crystallographic metal sites.

TABLE III. Hyperfine parameters for $Ni_2FeO_2BO_3$ measured at 300 and 115 K. ΔE_Q(mm/s) is the quadrupole splitting at the iron sites; δ_{Fe}(mm/s) is the isomer shift relative to $\alpha - Fe$; Γ (mm/s) is the linewidth at half height; A is the fraction of the total iron content in the site; B is the probability that the site is occupied by an iron ion (occupancy). Typical errors are $\pm 3\%$ on hyperfine parameters and $\pm 5\%$ on site occupancies.

T (K)	ΔE_Q	δ_{Fe}	Γ	A (%)	B (%)	Site
300	1.08	0.29	0.26	10	13.3	1
	1.28	0.34	0.31	30	40	2
	1.08	0.38	0.33	54	72	3
	1.93	0.35	0.34	6	8	4
110	1.10	0.44	0.26	8	10.7	1
	1.31	0.47	0.28	30	40	2
	1.09	0.50	0.38	55	73.3	3
	1.98	0.48	0.29	8	10.7	4

As temperature decreases, the paramagnetic pattern remains invariable down to 107 K, when a noticeable broadening of the peaks is clearly observed indicating relaxation effects. The spectrum taken at 110 K was fitted to four doublets whose hyperfine parameters are displayed in Table III. The quadrupole splittings measured at 300 K are clearly temperature independent down to 110 K while the isomer shifts show a small temperature dependence.

The spectrum taken at 105 K shows clear evidence of HFD. The evolution for further decreasing temperatures is characterized by an increase of the hyperfine magnet fields and a decrease of the distribution halfwidths centered at the most probable hyperfine field. All the spectra taken below 105 K show $p(H_M)$ curves comprising three distributions. As shown in Fig. 9, for 85 K and 4.2 K, these distributions are centered at 325 and 510 kOe. At 4.2 K the $p(H_M)$, with typical Fe^{3+} hyperfine fields in the range 400–510 kOe, is indicative that the system is very near the saturated state. At such temperature *all the iron ions are magnetically coupled*. The spectrum taken at 85 K represents an intermediate regime between the onset of the magnetic ordering ($T_{moss} \approx 106$ K) and the almost saturated state; the resulting $p(H_M)$, with three broad distributions, is consistent with such an intermediate regime. See Table IV.

The experimental curve for the iron reduced hyperfine field, $H_M(T)/H_M(4.2)$, as well as the theoretical reduced magnetization curves for S = 1 and S = $\frac{5}{2}$, obtained from the Brillouin theory, are shown in Fig. 10. For each temperature, $H_M(T)$ is the most probable hyperfine field value. The statistical counting error[19] on the hyperfine field, for our measurements, is less than 4 kOe, while the instrumental uncertainties, as estimated from a sample standard deviation,[19] is less than 1 kOe. Therefore, the error bars in Fig. 10 are smaller than the symbols. It is important to point out that, for $T \approx 46$ K, the temperature of the intense peak in the magnetic susceptibility, the curve for the iron reduced hyperfine field *does not show any anomaly*. We may conclude then that the iron subsystem is decoupled from the remaining Ni spins that in turn order at $T_N^{Ni} \approx 46$ K. The 3D nature of the magnetic ordering of the Fe subsystem at $T_N^{Fe} = 106$ K is indicated by the reasonably good fit of the reduced hyperfine field vs reduced temperature by the mean-field Brillouin function for

FIG. 9. (a) Mössbauer spectra taken at different temperatures below T_N^{Fe} from Ni$_2$FeO$_2$BO$_3$. (b) Hyperfine field distributions for the spectra shown.

FIG. 10. Iron reduced hyperfine fields vs reduced temperatures for Ni$_2$FeO$_2$BO$_3$ (circles). As mentioned in the text, the error bars are smaller than the symbols. The curves represent the theoretical reduced magnetizations, calculated from the Brillouin theory, for $S=1$ (dashed line) and $S = \frac{5}{2}$ (continuous line).

Fe and Ni subsystems. In the Mossbauer experiments this coupling shows up as an additional hyperfine contribution on the Fe nucleous giving rise to the small discontinuity in $H_M(T)$.

IV. DISCUSSION

Our magnetic measurements in Ni$_2$FeO$_2$BO$_3$ have shown three anomalies appearing at 15, 46, and 106 K, respectively. The last one, which appears as a weak peak in the ac susceptibility curve, is clearly associated with the ordering of the iron subsystem, since this corresponds to the temperature at which the Zeeman splitting in the Mossbauer spectrum disappears. The 3D character of this ordering may be inferred from Fig. 10 where it is seen that the iron reduced hyperfine field follows reasonably well the theoretical curve of the reduced magnetization obtained from the Brillouin theory. On the other hand, the spin-glass nature of this transition is suggested by the degree of dilution, the intrinsic randomness and the antiferromagnetic type of magnetic couplings of the Fe moments.[14] This is also consistent with the observation of history effects in the magnetization curves below 106 K.

The strong anomaly at 46 K, present in the χ_{ac} vs T curve, in the magnetization M vs T and M/H vs T curves is identified as the ordering temperature of the nickel subsystem. The antiferromagnetic nature of this ordering is inferred from the fact that this peak moves to lower temperatures as the applied field H increases and furthermore it shows no frequency dependence in the range from 20 to 1000 Hz. The peak or Néel temperature vs applied magnetic field, at low fields, is well described by the standard mean-field result for the shift of Néel temperature with applied field,[20] i.e., $T_p(H) = T_N^{\text{Ni}} - aH^2$, close to $T_N^{\text{Ni}} = 46$ K as shown in Fig. 7. Also, this agreement suggests the 3D nature of the antiferromagnetic transition since, if it occurred in lower dimensions, fluctuations would certainly be important and the mean-field result would not fit the experimental data.

$S = \frac{5}{2}$ as shown in Fig. 10. As concerns the type of magnetic ordering, it is most certainly a spin-glass rather than an antiferromagnetic transition.[14] This is suggested by the randomness in the position of the Fe magnetic moments and the antiferromagnetic character of their interactions. Unfortunately, this transition is barely visible in the ac susceptibility measurements since it is masked by the large susceptibility of the Ni ions. This makes it impossible to check, for example, for its frequency dependence. On the other hand the observation of history effects in the magnetization curves below 106 K as shown in Fig. 5, reinforces this point of view.

Finally, notice the existence of a discontinuity in the $H_M(T)$ curve at $T_N \approx 15$ K. This is the same temperature for which anomalies in the susceptibility curves occur. At this point it seems quite straightforward to associate these anomalies at 15 K with the magnetic coupling between the

TABLE IV. Hyperfine parameters for Ni$_2$FeO$_2$BO$_3$ measured at low temperatures. ΔE_Q is the quadrupole splitting at the iron sites; δ_{Fe} is the isomer shift relative to $\alpha-$Fe; Γ is the linewidth at half height for all the Lorentzian used in the fitting; $H_m ax$ is the most probable hyperfine field.

	110 K	85 K	4.2 K
$H_m ax$ (kOe)	235	335	510
ΔE_Q (mm/s)	-0.05	-0.04	-0.04
δ_{Fe} (mm/s)	0.49	0.48	0.50
Γ (mm/s)	0.34	0.38	0.37

The Fe and Ni subsystems are completely decoupled down to $T_N = 15$ K. The main evidence for that comes from the iron reduced hyperfine field vs temperature curve that does not show any anomaly at the nickel ordering temperature. Within this frame we interpret the anomaly that appears at 15 K in all magnetic measurements as indicative of the coupling between both subsystems. The temperature of this anomaly does not depend markedly on the applied magnetic field.

The picture above is in agreement with Goodenough rules[21] for cation-cation magnetic interactions in an oxide. Such rules predict a negligible value for the direct interaction between Ni^{2+} and Fe^{3+} if their coordination octahedra share a face or an edge as is the case in the ludwigites. Consequently, the interaction between different neighboring magnetic ions inside the same wall is due to superexchange that in the ludwigites is weak since the corresponding angle, Ni^{2+}-O^{2-}-Fe^{3+}, is near 90°.

Since both subsystems order, either antiferromagnetically or in a spin-glass arrangement, and as the intrasystem interactions are stronger than the intersystems, the material, as a whole, does not present a net magnetization if the applied field goes to zero.

At the beginning of our investigation we expected to observe two-dimensional magnetic behavior on the ludwigite. This was borne out from the existence of walls in these systems, where the magnetic ions are located. However, the only signature of low-dimensional effects we found is in the ac susceptibility for $T_N^{Ni} < T < T_N^{Fe}$. In this temperature range this quantity has a power-law behavior $\chi_{ac} \propto T^\alpha$ with $\alpha \approx -0.7$ typical of one-dimensional antiferromagnetic disordered Heisenberg chains as we have shown extensively in our previous studies of the warwickites.[7-9] As discussed in these references, this power-law behavior of the susceptibility, with $\alpha \approx -0.7$, is associated with the magnetic response of isolated disordered chains. In the present case, this result is interpreted as the response of the Ni chains before they couple together at T_N^{Ni} and the Ni subsystem, as a whole, orders antiferromagnetically in 3D. The results obtained above in fact allow us to understand why the walls are not relevant from the point of view of magnetic behavior. The reason is the negligible coupling between the Fe and Ni subsystems. Since there are sites along the walls with occupancies as high as, say 73% Fe, these *lines* of Fe *cut* the interactions among the Ni chains along the walls. Consequently, the magnetic crossover is from REHAC behavior directly to 3D antiferromagnetism.

ACKNOWLEDGMENTS

[1] R. Norrestam, Z. Kristallogr. **189**, 1 (1989).

[2] R. Norrestam, K. Nielsen, I. Sotofte, and N. Thorup, Z. Kristallogr. **189**, 33 (1989).

[3] Jan-Olov Bovin, M. O'Keeffe, and M. A. O'Keefe, Acta Crystallogr., Sect. A: Cryst. Phys., Diffr., Theor. Gen. Crystallogr. **37**, 28 (1981).

[4] J. O. Bovin, A. Carlsson, R. Sjövall, R. Thomasson, R. Norrestam, and I. Sotofte, Z. Kristallogr. **211**, 440 (1996).

[5] R. Norrestam, M. Kritikos, K. Nielsen, I. Sotofte, and N. Thorup, J. Solid State Chem. **111**, 217 (1994).

[6] J. J. Capponi, J. Chenavas, and J. C. Joubert, J. Solid State Chem. **7**, 49 (1973); J. J. Capponi, Thèse Docteur és-Sciences Physiques, L'Université Scientifique et Médicale de Grenoble, 1973.

[7] J. C. Fernandes, R. B. Guimarães, M. A. Continentino, H. A. Borges, J. V. Valarelli, and A. Lacerda, Phys. Rev. B **50**, 16 754 (1994).

[8] M. A. Continentino, J. C. Fernandes, R. B. Guimarães, B. Boechat, H. A. Borges, J. V. Valarelli, E. Haanappell, A. Lacerda, and P. R. J. Silva, Philos. Mag. B **73**, 601 (1996).

[9] M. Brunner, J. L. Tholence, L. Puech, S. Haan, J. J. Capponi, R. Calemczuk, J. C. Fernandes, and M. A. Continentino, Physica B **233**, 37 (1997).

[10] R. B. Guimarães, J. C. Fernandes, M. A. Continentino, H. A. Borges, C. S. Moura, J. B. M. de Cunha, and C. A. dos Santos, Phys. Rev. B **56**, 292 (1997).

[11] M. Matos, R. Hoffmann, A. Latge, and E. V. Anda, Chem. Mater. **8**, 2324 (1996).

[12] D. C. Marcucci, A. Latge, E. V. Anda, M. Matos, and J. C. Fernandes, Phys. Rev. B **56**, 3672 (1997).

[13] J. Dumas, M. A. Continentino, J. J. Capponi, and J-L. Tholence, Solid State Commun. **106**, 35 (1998).

[14] H. Neuendorf and W. Gunβer, J. Magn. Magn. Mater. **173**, 117 (1997); A. Wiedenmann, P. Burlet, and R. Chevalier *ibid.* **15-18**, 218 (1980).

[15] S. A. De Waal E. A. Viljoen, and L. C. Calk, Trans. Geol. Soc. S. Afr. **77**, 375 (1974).

[16] J. Rodriguez-Carvajal, *Short reference guide of the program* FULLPROF (1997). Version 3.2 available in ''pub/divers/fullp'' of the anonymous ftp area of the LLB unix cluster.

[17] B. Window, J. Phys. C **3**, S323 (1970); J. Phys. E **4**, 401 (1971).

[18] H. Keller and I. Savić, Phys. Rev. B **28**, 2638 (1983).

[19] P. R. Bevington, *Data Reduction and Error Analysis for the Physical Sciences* (McGraw-Hill, New York, 1969).

[20] S. M. de Oliveira, P. M. de Oliveira, and M. A. Continentino, Physica A **152**, 477 (1988), and references therein.

[21] J. B. Goodenough, Phys. Rev. **117**, 1442 (1960).